Ceramics International 45 (2019) 18751–18759

Contents lists available at ScienceDirect

Ceramics International

journal homepage: www.elsevier.com/locate/ceramint

In-situ measurements of high-temperature dielectric properties of municipal solid waste incinerator bottom ash

Georgia Flesoura[a,*], Beatriz Garcia-Banos[b], Jose M. Catala-Civera[b], Jef Vleugels[a], Yiannis Pontikes[a]

[a] KU Leuven, Department of Materials Engineering, Kasteelpark Arenberg 44, 3001, Heverlee, Belgium
[b] ITACA Institute, Universitat Politècnica de València, Camino de Vera s/n, Valencia, 46022, Spain

ARTICLE INFO

Keywords:
Dielectric properties
Microwave processing
MSWI bottom ash

ABSTRACT

Microwave heating is a potential green technology demonstrating many advantages over conventional heating methods. Prior to designing an industrial microwave process, however, a fundamental knowledge of the dielectric properties of the material to be thermally treated is imperative, as these properties determine the response of the material to an applied electromagnetic field. In this study, the fundamental interactions between microwave energy and municipal solid waste incinerator (MSWI) bottom ash (BA) are investigated through in-situ complex permittivity measurements. Using an enhanced version of the cavity perturbation method, the dielectric properties were determined from room temperature up to 1100 °C at a frequency close to the industrial 2.45 GHz. The results demonstrated that BA is a low-loss microwave absorber up to 320 °C, above which microwave flash pyrolysis of the organic matter abruptly enhances the dielectric loss of BA, resulting in a thermal runaway. The addition of water and graphite to BA induces a higher dielectric constant and loss factor. The evolution of the dielectric properties as a function of temperature is correlated to changes in the material as determined by Simultaneous Differential Scanning Calorimetry, Thermogravimetric Analysis and High Temperature X-ray Diffraction. The reported results form a baseline for the assessment of the MSWI BA response under microwave irradiation.

1. Introduction

Global population growth along with the ever-increasing standard of living, results in resource depletion and the generation of large amounts of municipal waste. The social, environmental and health impacts associated with the disposal of waste in landfills have prompted the European Commission to implement solid waste prevention and management policies. The Waste Framework Directive relies on a waste hierarchy that includes in order of priority: prevention, preparation for use, recycling, other recovery (e.g. energy recovery achievable by the incineration of waste) and disposal [1].

The major types of waste subjected to incineration are municipal waste, non-hazardous industrial, hazardous, and medical waste, as well as sewage sludges [2]. Through the incineration process heat is generated, recovered and converted into energy. Simultaneously, the process itself contributes to the breakdown of pollutants and waste volume reduction [3]. Incineration leads also to the generation of BA. Currently, BA is used as embankment filler, landfill structure material, road subbase material and aggregate in concrete [4]. A straightforward alternative approach in terms of circular economy is the utilization of BA in building materials. The presence of heavy metals in BA, however, is considered to be one of the main hindrances to its direct use. Acknowledging that, a significant amount of research has been undertaken related to beneficiation techniques for the use of BA as raw material for different applications. Among the metal extraction techniques, washing and ageing are already implemented at industrial scale, whereas vitrification has drawn research attention and emerges as the most effective technique for high immobilization efficiency of heavy metals [5]. Nevertheless, vitrification entails a high temperature operation and is considered a non-economical route because of the high energy consumption [6].

In response to this, a novel and potential green technology, which has demonstrated advantages over conventional heating methods, is microwave heating. The ability of microwaves to heat selectively, and quite often volumetrically, depending on the microwave process equipment, results in high heating rates and energy savings. These essential features favor its selection in many processes, such as waste treatment and vitrification [7]. One such example is the sintering of BA

* Corresponding author.
E-mail address: georgia.flesoura@kuleuven.be (G. Flesoura).

https://doi.org/10.1016/j.ceramint.2019.06.101
Received 18 March 2019; Received in revised form 18 May 2019; Accepted 11 June 2019
Available online 12 June 2019

into ceramic bricks by Taurino et al. using hybrid microwave processing, where BA was found to be a poor microwave absorber [8].

However, prior to processing any material under microwave irradiation, a fundamental knowledge of the dielectric properties is imperative. These properties offer essential information and guidance about the response of the material during processing, the microwave penetration depth and whether a material will absorb, reflect or transmit the microwaves at a particular temperature. Furthermore, microwave process simulation for upscaling and optimization is only possible when the governing dielectric properties are known [9].

Ashes and slags are complex materials with different compounds that interact with each other and the electromagnetic field. These compounds will affect the dielectric response of the bulk material, as the dielectric properties are also dependent on moisture content, density, chemical and physical composition, crystal structure and temperature [10,11]. This implies that the synergy of the compounds will have an influence on the heating efficiency of the microwave process.

In the field of MSWI BA, studies on microwave processing are limited. One example is the work of Aamir Ilyas et al. [12], who studied the dielectric permittivity of BA at room temperature and a frequency between 300 MHz and 1.5 GHz, as a function of the volumetric water content (VWC), aiming to develop a microwave based non-invasive emission monitoring and control system to measure the moisture content of BA. A linear relationship between the dielectric permittivity and the water content was measured, which permits the estimation of the latter by means of the dielectric permittivity.

As one can see in this work and others, the dielectric properties are measured at room or near room temperature. When aiming to assess the materials´dielectric response, it is important to recognize that they are frequency and temperature dependent. Consequently, the material dielectric response evaluation has to be performed within the targeted temperature and frequency range of interest.

To the best of our knowledge, no study has been carried out to evaluate the MSWI BA microwave response, and the lack of fundamental understanding of the BA behavior at industrial frequency and high temperatures is an impediment to effectively design pilot and upscale microwave processes.

The aim of this paper is to evaluate the possibility of heating BA by microwave irradiation, by measuring the dielectric properties as a function of temperature and at a frequency close to the industrial 2.45 GHz, and calculating the microwave penetration depth. Initially, the dielectric properties of the dry BA (DBA) are presented. Simultaneously, the authors explored the addition of water and graphite to BA (WBA), which have a tangible effect on the overall complex permittivity of the material and heating efficiency of the microwave process. The evolution of the dielectric properties with temperature are compared with the results of thermo-analytical techniques and High Temperature X-ray diffraction (HT-XRD).

2. Experimental

2.1. Materials and methods

MSWI BA was supplied by Heros Sluiskil B.V. (The Netherlands). After the incineration process, quenching (fast cooling) in water followed, with subsequent removal of ferrous and non-ferrous metals. The BA was then piled up in atmospheric environment for 2–3 months for stabilization purposes. Small samples were dried in a laboratory oven at 105 °C until no change in weight could be recorded, before determination of the chemical, mineralogical, thermo-analytical and dielectric response. MSWI BA samples were initially crushed in a disk mill (Retsch DM200), followed by milling in a vibratory ring mill (Retsch RS200) to a particle size < 100 μm. These samples are referred to as DBA. In the WBA samples, 2 wt% of additional carbon (graphite powder, Alfa Aesar, purity 99.9%) was added and the mixture was dry mixed with Al_2O_3 (Ø10 mm) milling balls on a multidirectional Turbula mixer (WAB, Switzerland) for 8 h to guarantee a homogeneous mixing. WBA samples were afterwards wetted with MilliQ water (resistivity 18.2 MΩ) to obtain a 25 wt% moisture content, similar to the fresh as-received BA material (due to in-plant quenching) [13].

A nitrogen gas pycnometer (Quantachrome, MVP-6DC) was used to determine the real density of the BA powder. The chemical composition was determined using a Bruker S8 TIGER 4 kW sequential WD-XRF spectrometer with rhodium anode, using the Quant Express software.

Simultaneous Differential Scanning Calorimetry and Thermogravimetric Analysis (SDT) were used to determine the heat flow and weight changes of MSWI BA as a function of temperature. For the SDT experiments (SDT Q600, TA instruments), 200 mg of MSWI BA was heated in an alumina sample holder, with a heating rate of 10 °C/min, under a flow of nitrogen (50 ml/min) in the temperature range of 25 °C–1200 °C.

High Temperature X-ray Diffraction (HT-XRD) was performed on a θ-θ diffractometer (3003-TT, Seifert, Ahrensburg, Germany), using Cu K_α radiation (40 kV, 30 mA), with a parabolic multilayer mirror for parallel beam optics. This reduces the susceptibility to thermally induced sample position changes, and a long 0.4° collimator in front of the scintillation detector was used to increase the angular resolution [14]. Room temperature XRD was performed using the same device. For the HT-XRD measurements, an X-Ray furnace (HDK 2.4, Johanna Otto, Hechingen, Germany) was used, with a Mo heating element, surrounding the sample under a flow of nitrogen (100 ml/min) between room temperature and 1100 °C, with a heating rate of 10 °C/min. A pressed BA pellet was used to avoid contamination of the furnace during heating. Diffraction spectra were acquired at room temperature and from 300 °C to 1100 °C at 100 °C intervals during heating. The data were obtained in the 2θ range from 10° to 70° (step width 0.04°, measurement time = 15 min/step). For quantification of the mineral phases at room temperature and estimation of the amorphous content, 10 wt% of analytical grade crystalline ZnO was added to DBA as a standard material. The mixture was milled for 7.5 min in a McCrone micronizing mill using ethanol (purity 99.9%) as a grinding agent and corundum grinding elements to ascertain sufficient fineness for analysis. Diffraction patterns were obtained in the 10°–70° 2θ range using Cu K_α radiation (40 kV, 30 mA) and a step size of 0.04°. The acquired data were evaluated with EVA V.3.1 (Bruker AXS) and quantified with Topas Academic V.5 [15], using the Rietveld method in combination with the fundamental parameter approach. The ICSD database was used for the structural data [16]. Rietveld analysis was also carried out to quantify the individual mineral phases found by HT-XRD analysis, and the absolute weight percentages were obtained by MAUD V.2.8 Rietveld analysis.

Thermodynamic calculations were also carried out using the thermodynamic software package FactSage V.6.4, using FactPS and FTOxid databases, in order to calculate the minimum temperature of molten phase formation based on the XRF composition data of DBA. Determination of the total carbon (TC) content in DBA was performed by a Coulomat 702 SO/CS (Strohlein GmbH, Kaarst, F.R.G.) and the loss on ignition (LOI) according to the EN 14346 procedure.

2.2. Dielectric properties measurements

MSWI BA samples were measured within the temperature range of 25 °C to almost 1100 °C under continuous flow of nitrogen (50 ml/min), in order to avoid oxidation or combustion. Each sample consisted of a volume of 1.13 ml of BA, and the measurements were repeated at least three times to ensure that the results were representative of the actual behavior of the material. Samples were placed inside a quartz holder, which was inserted in a cylindrical waveguide microwave system (Fig. 1) [17,18].

The latter consists of a cylindrical cavity (diameter 104.92 mm and 85 mm height). The cavity operates simultaneously in two modes, i.e., TE111 for heating the sample and TM010 for measuring its dielectric

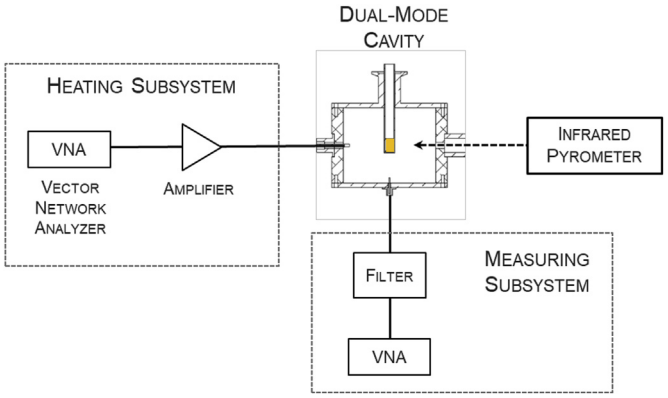

Fig. 1. Schematic of the microwave system for heating and dielectric characterization of the DBA and WBA samples.

properties. Each subsystem works independently and a cross-coupling filter avoids any interference between the heating signal and the measurement signal.

The heating signal is generated by a Vector Network Analyzer (VNA) that delivers an output of 1 mW (0 dBm), followed by an amplifier with a gain of 50 dB, delivering to the cavity a maximum power of 150 W. The heating signal is launched into the cavity through a high-power coaxial cable connected to an electric probe penetrating a variable distance into the cavity through the sidewall.

The resonance of the heating mode varies as a consequence of the temperature dependence of the dielectric properties of the sample. This means that the heating signal needs certain adjustment to ensure the desired heating rate during the process. The VNA signal has a certain bandwidth that can be continuously adjusted to track the resonant peak of the heating mode. In addition, the penetration of the electric probe at the side wall modifies the amount of power applied to the sample. A control software implemented in LabView, with a PID algorithm, allows automatic adjustment of these parameters to obtain the desired heating rate of the sample.

The low power measurement signal (1 mW) is generated by a second VNA, and coupled to the cavity by a second electric probe located at the bottom wall. This signal is monitored to determine the main parameters of the measurement resonance, which are the resonance frequency and the quality factor. From this measurement, and applying the cavity perturbation method (CPM) [18] the dielectric properties of the sample are obtained. The CPM is one of the most popular methods to determine dielectric properties of samples [17]. It relates the dielectric constant and the loss factor of a homogeneous and isotropic material to the shift in the resonance frequency and the change in the quality factor as follows:

$$\varepsilon' = 1 + \frac{-\Delta f\,(\eta + N\Delta f) - N\,(\Delta Q)^2}{(\eta + N\Delta f)^2 + N^2\,(\Delta Q)^2} \quad (1)$$

$$\varepsilon'' = \frac{\eta \Delta Q}{(\eta + N\Delta f)^2 + N^2\,(\Delta Q)^2} \quad (2)$$

Where Δf and ΔQ represent the shift in resonance frequency and quality factor, when the sample is placed in the measurement cavity with respect to the values when the cavity is empty. The parameters are the sample filling factor and the sample depolarization factor respectively and they are empirically obtained through a calibration process [17,18]. A detailed explanation of the method can be found elsewhere [17,18]. Thus, the cavity perturbation method (CPM) entails a continuous measurement of the resonant frequency and quality factor in the cavity as a function of temperature. By means of this procedure, the accuracy of the dielectric constant and loss factor has been estimated to be 3% and 10% respectively [18].

The cavity is designed with two holes in the side walls, one for sample inspection with a video camera and one for temperature measurements with an IR pyrometer (with an accuracy of 0.1ºC). It should be noted that the IR pyrometer points to the surface of the quartz holder, hence a calibration method [18] is applied to obtain the bulk temperature of the sample from this measurement.

Table 1
Normalized chemical composition of DBA, based on XRF data (relative error of semi quantitative analysis: 10%).

Compound	% wt
SiO_2	48
CaO	18
Fe_2O_3	10
Al_2O_3	9
MgO	2
TiO_2	1
LOI	7.5
Total Carbon (TC)	3

3. Results and discussion

3.1. Characterization of BA

The chemical composition of DBA is presented in Table 1 and predominantly consists of SiO_2 followed by CaO, Al_2O_3 and Fe_2O_3, as well as minor quantities of MgO and TiO_2. Table 2 provides the quantification of the mineral phases present in DBA at room temperature.

3.2. Evaluation of dielectric properties of DBA

Fig. 2 presents the measured dielectric properties of DBA in the 25°C–1062 °C range. The measurement was stopped at 1062 °C because of the limited maximum power input of 150 W. The dielectric properties evolution of DBA as a function of temperature can be divided into three distinct temperature zones. The first zone is characterized by drying, where the response of DBA up to 320 °C is confined to low dielectric constant and dielectric loss factor values. This corresponds to the low and constant heating rate of DBA, presented in Fig. 3.

The continuous temperature increase gave rise to an abrupt and considerable change in dielectric properties around 320 °C, attributed to a thermo-chemical conversion, i.e., pyrolysis of organic matter in the material. The synergy between the material's increased absorption of microwave energy and temperature increase results in a thermal runaway up to 820 °C. Above that temperature, structural changes taking place in the DBA notably influence the dielectric properties, i.e., the dielectric loss factor continuously rises until the completion of microwave processing at 1062 °C, whereas the dielectric constant reached a maximum around 950 °C.

Heating from 25 °C to 320 °C occurs at a constant rate of 10 °C/min, whereas the temperature instantaneously increases from 320 °C to 820 °C within 1 min. At higher temperatures, heating continues at 30 °C/min, as shown in Fig. 3. The total heating time to reach 1062 °C

Table 2
Mineralogical composition of DBA (estimated relative error: 10%).

Phase	Chemical composition	wt%
Calcite	$CaCO_3$	3.4
Clinopyroxene (clinoenstatite)	$MgSiO_3$	9.3
Hematite	Fe_2O_3	0.9
Melilite (gehlenite)	$Ca_2Al(Al_2SiO_7)$	2.2
Plagioclase feldspar (anorthite)	$CaAl_2Si_2O_8$	0.6
Quartz	SiO_2	14.4
Amorphous/not detected		69.2

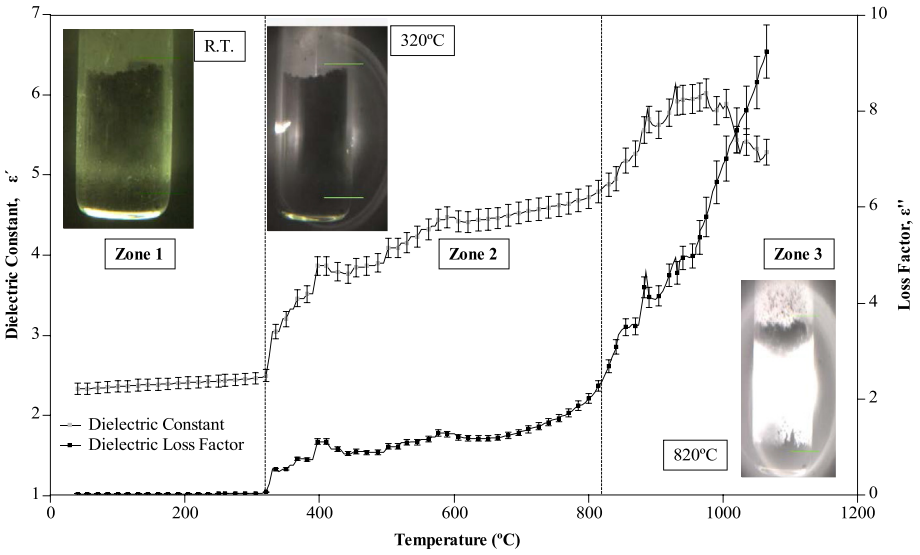

Fig. 2. Measured dielectric properties of DBA as a function of temperature. The images in each temperature range, depict the photos of DBA taken by the video camera during the dielectric properties measurements.

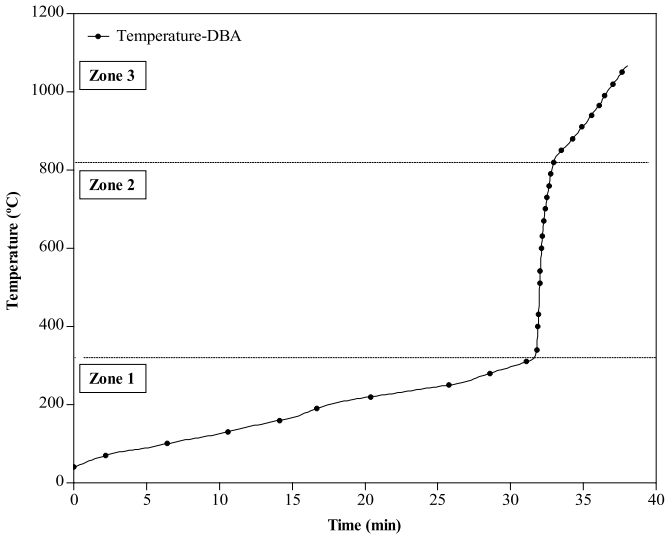

Fig. 3. Temperature profile of DBA during dielectric properties measurement with an increasing power input up to 120 W.

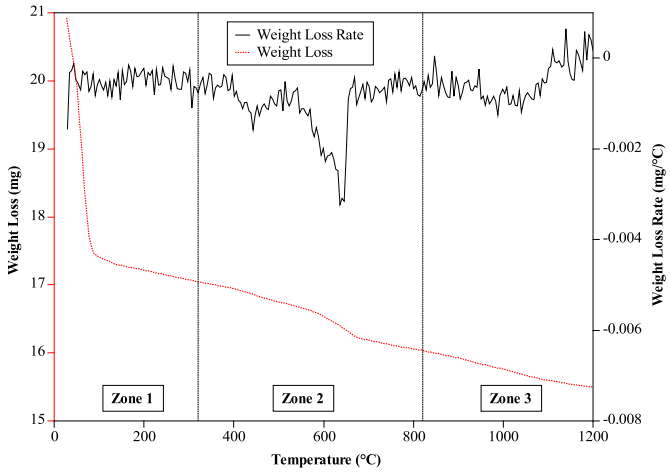

Fig. 4. Thermogravimetrical analysis (TGA) (dotted-red line) and its first derivative (continuous-blackline) of DBA. (For interpretation of the references to colour in this figure legend, the reader is referred to the Web version of this article.)

was almost 40 min.

To gain a better insight into the underlying phenomena affecting the dielectric properties and concomitant microwave response of DBA, three distinct temperature regions can be differentiated, as analyzed in more detail by SDT (see Fig. 5). The evolution of the mineralogy as a function of temperature during HT-XRD, as determined by MAUD software analysis, is shown in Fig. 6. The calculations do not consider the presence of amorphous phases or the formation of molten phases, and reflect only the relative crystalline phase content. As shown in Fig. 6, the quartz content is significantly reduced with increasing temperature and completely disappears at 1100 °C. Quartz (SiO_2), calcite ($CaCO_3$), hematite (Fe_2O_3), gehlenite ($Ca_2Al(Al_2SiO_7)$) and anorthite ($CaAlSi_2O_8$) are transformed into pyroxene minerals, such as hedenbergite ($CaFeSi_2O_6$), diopside ($CaMgSi_2O_6$) and clinoenstatite ($MgSiO_3$), together with albite ($NaAlSi_3O_8$), akermanite ($Ca_2Mg(Si_2O_7)$) and low quantities of wüstite (FeO) and metallic iron (Fe).

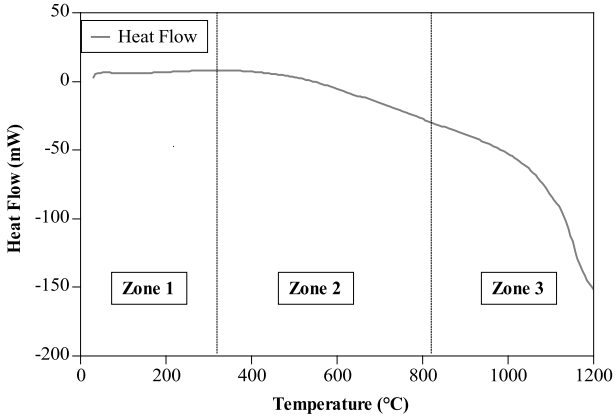

Fig. 5. Differential scanning calorimetry (DSC) curve of DBA.

3.2.1. Zone 1: temperature range 25 °C–320 °C

Since the loss factor is almost constant (at least with the scale used in Fig. 2), the temperature slightly increases up to 320 °C, where ε´´ reaches a value of 0.13. The temperature increase is accompanied by a weight loss, as shown in the TGA curve in Fig. 4.

Since significant temperature gradients can exist even in a small

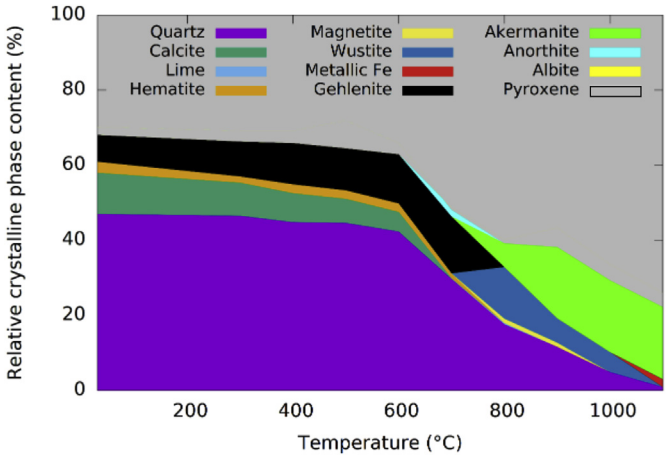

Fig. 6. Calculated evolution of the relative amount of crystalline phases in the DBA as a function of temperature.

amount of microwave heated material, it is assumed that the phenomena arising during dielectric property measurements precede the pyrometer temperature measurements [19–21]. Moreover, the temperature gradient is opposite during microwave heating compared to conventional heating, with the highest temperature in the center of the sample and not on the surface, resulting in higher bulk temperature during the dielectric property measurements than indicated by the pyrometer. This complicates a direct correlation between the evolution of the dielectric properties (Fig. 2) and the weight loss and heat flow curves (Figs. 4 and 5).

No mineralogical changes were detected by XRD analysis up to 300 °C, as shown in Fig. 7. The main mineral phases found in DBA at room temperature are quartz (SiO_2), plagioclase feldspars (mainly anorthite, $CaAl_2Si_2O_8$), calcite ($CaCO_3$), clinopyroxene (mainly clinoenstatite ($MgSiO_3$), melilites (mainly gehlenite ($Ca_2Al(Al_2SiO_7)$) and hematite (Fe_2O_3). This composition is in accordance with those reported by other researchers [2,22].

The heating rate of DBA in the 25–320 °C range is almost linear and around 10 °C/min, accompanied by a weight loss rate that can be correlated with the loss of physically and chemically bound water. The small change in dielectric properties in this temperature region should be directly related to the changing chemical structure, i.e. increased ionic strength of the residual amount of bound water in the DBA.

3.2.2. Zone 2: temperature range 320 °C–820 °C

Both the dielectric constant and loss factor undergo a discernible increase, which is associated with the pyrolysis of organic matter and the beginning of char production. In this temperature range, the light volatile gases are released, as confirmed by the fumes on the picture taken at 320 °C in Fig. 2. Tar is also released without necessarily affecting the dielectric properties. However, the release of volatiles is responsible for the production of solid char. Above 320 °C, the electric field induces motion of the charges of the resulted solid char dissipating energy in the form of heat due to the Maxwell-Wagner or Interfacial polarization effect. Once pyrolysis starts, consecutive microwave absorption takes place as confirmed by the increasing ε′ and ε′′, reaching values of respectively 4.8 and 2.4 at 820 °C.

Microwave pyrolysis has also been reported by other researchers as the initiation of dielectric heating [23]. Char produced above 550 °C is known as a microwave receptive additive that further promotes microwave pyrolysis [24]. This leads to the formation of hot spots, i.e. regions of the bulk material that exhibit higher temperatures, inducing local conductive heating. The high temperature of 820 °C achieved within almost 1 min can be referred to as a thermal runaway effect that was triggered by the pyrolysis of organic matter and which results in a microwave flash pyrolysis process.

Simultaneously, other thermochemical conversions took place within the aforementioned temperature range. Iron oxide in the form of

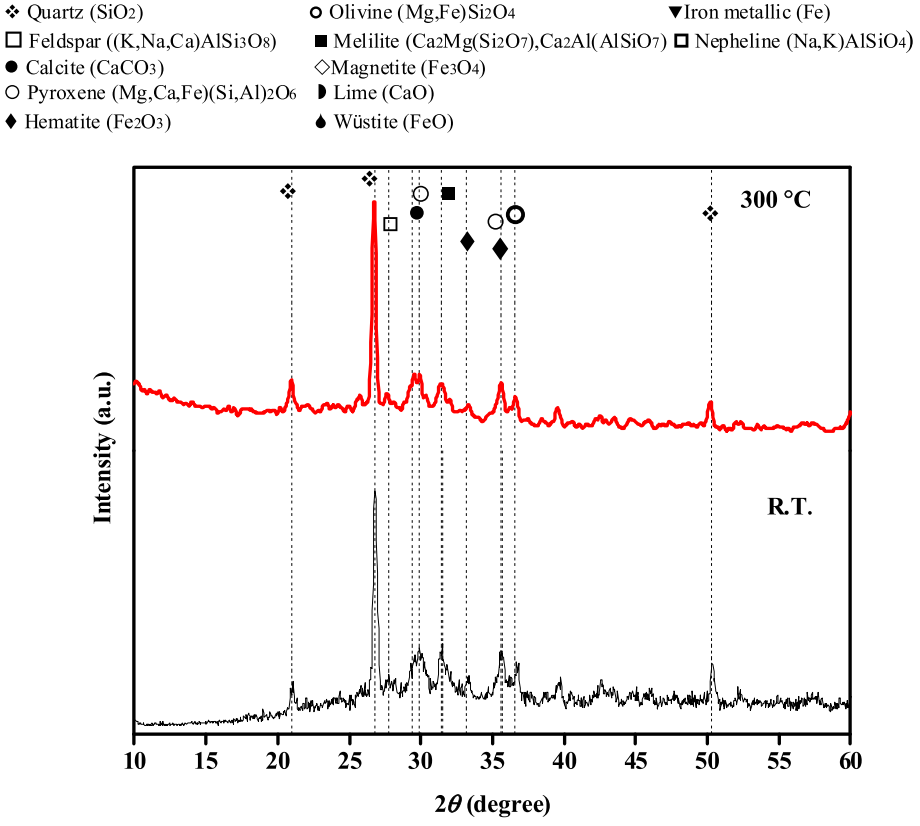

Fig. 7. Comparison of the XRD patterns of DBA as a function of temperature.

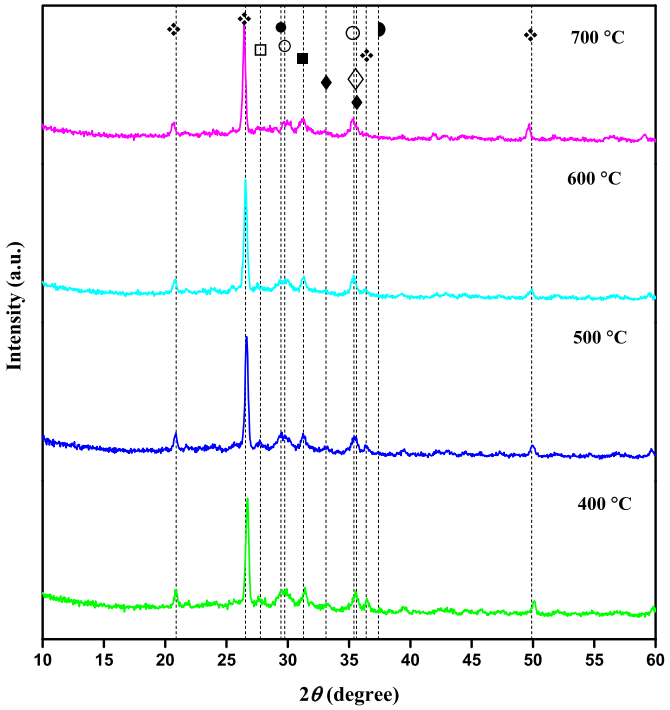

Fig. 8. Comparison of the XRD patterns of DBA from 400 °C to 700 °C (the symbols of the mineral phases correspond to those in Fig. 6).

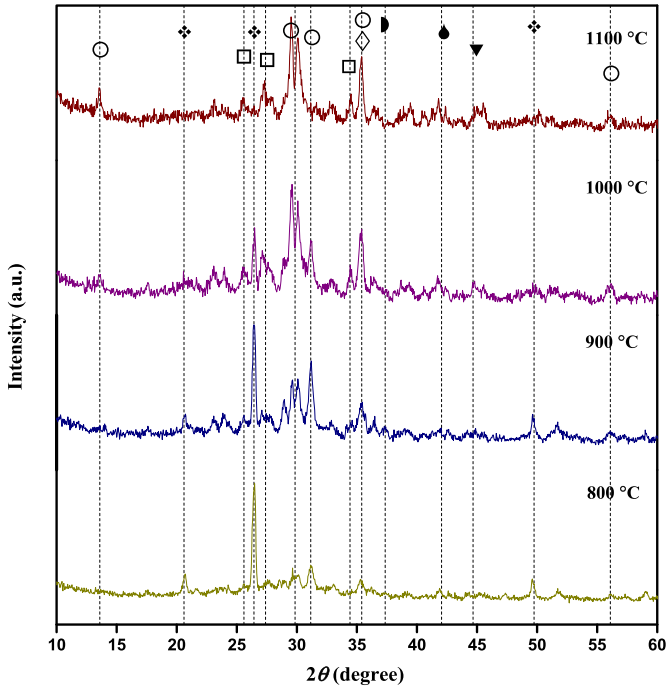

Fig. 9. Comparison of the XRD patterns of DBA from 800 °C to 1100 °C (the symbols of the mineral phases correspond to those in Fig. 6).

hematite (Fe_2O_3), as revealed by the room temperature XRD pattern (Fig. 6), was carbothermally reduced to magnetite (Fe_3O_4) between 700 °C and 800 °C, as confirmed in Fig. 6 and 6 and 7. Further reduction of Fe_3O_4 is revealed by the existence of the wüstite (FeO) peak at 800 °C. Hotta et al. [25] measured the permittivity of α-Fe_2O_3, Fe_3O_4 and Fe_xO powders using the coaxial transmission line method over a microwave frequency range between 0.2 and 13.5 GHz. The results at 2.45 GHz showed that the dielectric constant values for Fe_xO were larger than those of Fe_3O_4 and α-Fe_2O_3, implying an additional contribution of FeO to the bulk microwave absorption in the present work. McGill et al. [26] heated a wide range of powdered minerals in a microwave oven operating at 2.45 GHz with an incident power of 3 kW. The results revealed that Fe_3O_4 is an extremely good microwave absorber, reaching a temperature higher than 1000 °C in less than 1 min. Concurrently, at 700 °C, anorthite ($CaAl_2Si_2O_8$) was converted into the low-loss albite ($NaAlSi_3O_8$) [27], as can be observed in Figs. 6 and 8. The DTG curve (Fig. 4) exhibits a peak at 670 °C, where the weight loss is equal to 1.4% and attributed to the decomposition of calcite ($CaCO_3$) into lime (CaO) and carbon dioxide (CO_2) as confirmed by the XRD analysis in Figs. 6 and 8. According to the XRD patterns, $CaCO_3$ decomposition and CaO formation starts at 700 °C and finishes at 800 °C. In the same study by McGill et al. [26], CaO powder was heated for 1 min at 3 kW reaching a maximum temperature of 73 °C, implying CaO is a poor microwave absorber.

3.2.3. Zone 3: temperature range 820 °C–1062 °C

The step change in the dielectric loss factor at 820 °C signifies the continuous increase in dielectric properties and concomitant temperature. Several phenomena accompany the increase in temperature above 820 °C, as reflected in the complex evolution of the dielectric properties.

The significant transformation of mineral phases is associated with changes in the dielectric properties, without however providing an explanation for their increase. The intensity of the quartz (SiO_2) peaks decreased above 800 °C and completely disappeared at 1100 °C, due to its dissolution in the liquid phase. In addition, above 800 °C, gehlenite is replaced by akermanite and the majority of mineral phases were substituted by pyroxene group minerals, such as diopside ($MgCaSi_2O_6$), clinoenstatite ($MgSiO_3$) and hedenbergite ($CaFeSi_2O_6$). They have all been reported as low-loss dielectric minerals [27].

Concurrently, a complete reduction of Fe_3O_4 occurs at 900 °C producing exclusively FeO, which is subsequently reduced to Fe, the existence of which is disclosed by the appearance of the characteristic diffraction peaks in the XRD patterns at 1000 °C and 1100 °C (Fig. 9). The Fe particles, which have high electrical conductivity [28], increase the dielectric constant up to a maximum around 900 °C. Beyond that point, the authors assume that the dielectric constant decreases again due to reflection by coarsening and agglomeration of the Fe particles in the amorphous melt. However, the dielectric loss factor increases because of the Joule heating that rises by the induced eddy current on the metal surface [29]. However, the mobility of the free electron charges in the Fe product produces heat and this is clearly reflected in an increased ε′′ in Fig. 2.

The heat flow evolution in the DSC graph undergoes a sharp decrease, ending up in an endothermal peak that starts at 1140 °C, demonstrating the onset temperature of melting of DBA. FactSage calculations revealed that 34 wt% of DBA is already molten at 1100 °C. Assuming that the temperature in the middle of the sample is higher than the one measured by the pyrometer on the surface, melting of DBA is marked by a considerable and sudden increase in the dielectric loss factor and dielectric constant. The sudden slope increase of both loss factor and dielectric constant between 880 °C and 930 °C (see Fig. 2) can therefore be attributed to the onset of melting of DBA. Both dielectric parameters reach the highest values, with a loss factor of 9.5 at 1062 °C. When molten phases are present, the dipoles in the silicate melt have greater freedom to be polarized by the alternating electric field, introducing ionic conductivity and the dipolar polarization phenomenon. Hence, the increased mobility of the bound charges, induced by the electric field, gives rise to higher microwave absorption [30].

The dielectric constant shows a clear maximum around 930 °C, which could be due to the fact that the formed Fe particles rapidly coarsen/coagulate in the melt at higher temperatures, resulting in an enhanced microwave reflecting character.

The dielectric loss factor within zone 3 increases more rapidly than

the dielectric constant, which can be explained as a combined effect of the increase in electronic conduction due to Fe particle formation, and a concurrent increase in ionic conduction due to the mobility of the ions in the melt. These phenomena have a more prominent effect on the dielectric loss factor, while there is hardly any effect on the dielectric constant [31,32].

3.3. Evaluation of the dielectric properties of WBA

With the aim of enhancing the dielectric losses to reduce the processing time for DBA, especially within the temperature range up to 320 °C, the influence of an additional 2 wt% of graphite was investigated. Many researchers have used microwave absorbing materials, such as biochar, activated carbon and graphite to induce the pyrolysis reactions [23,31]. These additives act as susceptors, i.e. heating sources, that have the ability to readily absorb electromagnetic energy and convert it to heat at room temperature.

For the WBA material, 2 wt % graphite powder was mixed into DBA along with 25 wt% water in order to replicate the fresh bottom ashes produced after quenching of the combusted ash in the incineration plant. In the interest of comparison between the DBA and WBA dielectric response, the same distinct temperature ranges were used for the analysis of the results.

3.3.1. Zone 1: temperature range 25 °C–320 °C

The values of ε′ and ε′′ (see Fig. 10) are noted to increase significantly from room temperature and up to 117 °C, where ε′′ rised to 3.83. This is linked to the presence of water, which is selectively heated by the microwaves. Water is a strong microwave absorber with an ε′ = 80 at room temperature and 2.45 GHz [33], and when mixed with a material it amplifies the interaction between the latter and the electromagnetic field by introducing additional polarization [34]. The subsequent evaporation of water reduces the loss factor almost equally to the value of DBA at room temperature.

Apart from the contribution of water addition to the microwave heating efficiency at lower temperature, the graphite powder also provides high coupling efficiency, which is associated with a higher polarizability, as reflected by the increased dielectric constant values. The evolution of both loss factor and dielectric constant signifies that the microwave pyrolysis process that occurs at 320 °C in DBA is triggered earlier in WBA due to the graphite addition. This is confirmed by the temperature profile of DBA with 25 wt% water addition (see Fig. 12), where DBA needs almost 25 min to reach the temperature of 320 °C, showing the effect of water only up to 135 °C, when it evaporates. The increased heating rate and efficiency of WBA should therefore be attributed to the graphite addition. The high heating rate is a possible consequence of the effect of plasma formation, taking place when the charges of graphite are ionized and obtain augmented kinetic energy. An ionizing atmosphere surrounding the material could be created, which is reenacted as small regions of electric arc formation

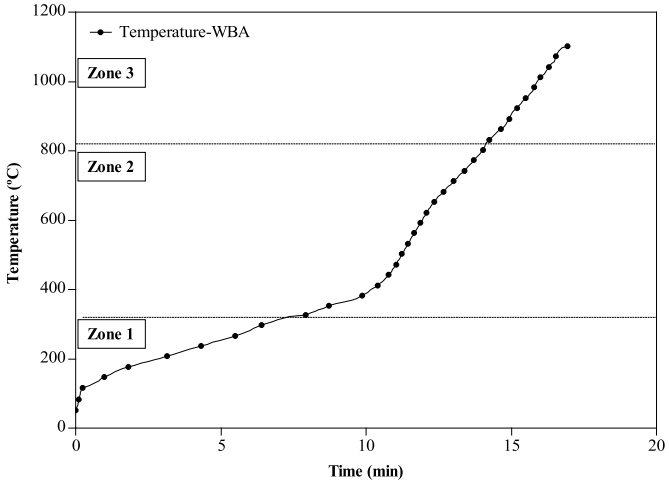

Fig. 11. Temperature profile of WBA during dielectric properties measurements.

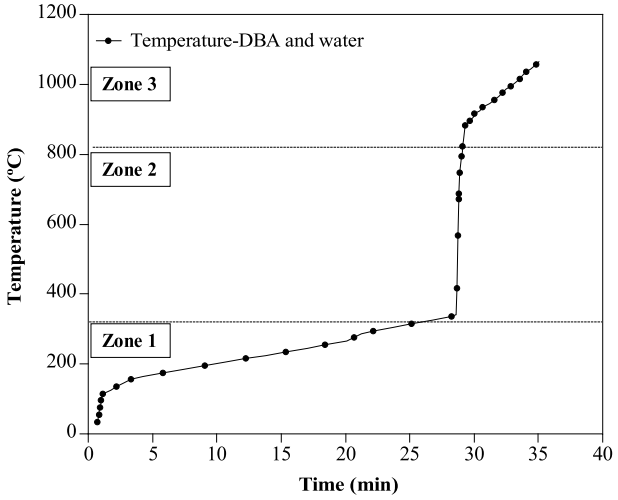

Fig. 12. Temperature profile of DBA with 25 %wt water addition during dielectric properties measurements.

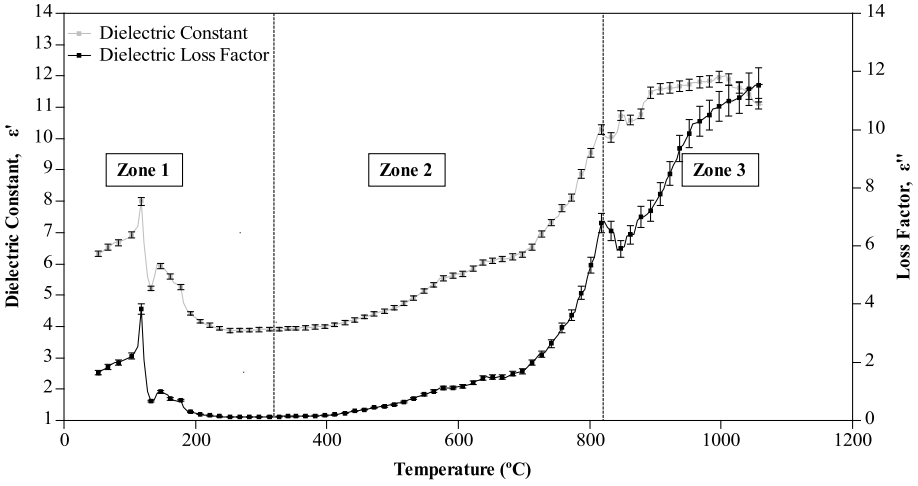

Fig. 10. Dielectric properties of WBA, measured as a function of temperature.

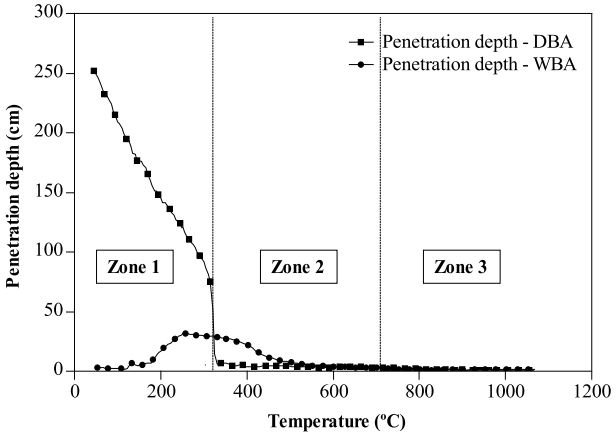

Fig. 13. Evolution of the penetration depth of 2.45 GHz microwaves in DBA and WBA material as a function of temperature.

inside the material, causing plasma [31]. It is worth mentioning that the processing time up to 200 °C is substantially reduced by water and graphite addition and accounts for 3 min, compared to 7 min for DBA with water addition and 17 min for DBA.

3.3.2. Zone 2: temperature range 320 °C–820 °C

While the heating profile of DBA in this temperature range is clearly dominated by a thermal runaway effect, heating of WBA increases linearly at 72 °C/min (see Fig. 11), and can be defined as controlled heating. The enhanced polarizability due to graphite addition is evident by the higher ε´´ of WBA compared to DBA, across the entire temperature range. In contrast to the increased dielectric constant, the dielectric loss factor for DBA is higher up to 600 °C (see Fig. 2). Graphite increases the electrical conductivity in WBA, which results in an amplified polarization but decreased dielectric loss compared to DBA. Nevertheless, above 600 °C the loss factor for WBA reaches higher values than DBA. As the temperature rises, there is a smooth transition followed by a continuous increase in both ε´ and ε´´ for WBA. This can only be attributed to the effect of the graphite addition on the pyrolysis reactions, which becomes more progressive in time instead of instantaneous. This evolution is also clearly reflected in the temperature profile difference of DBA (Fig. 3) and WBA (Fig. 11). Ultimately, DBA, which acts as a dielectric insulator, is transformed into an electrical semi-conductor (WBA) by increasing the overall carbon content. The distribution of carbon will define whether there is flash, controlled or even no increased heating rate, in case of a too high electrical conductivity, where the material will act as a reflector for electromagnetic waves.

3.3.3. Zone 3: temperature range 820 °C–1062 °C

In addition to the phenomena observed in this temperature range for DBA, the graphite addition in WBA results in an enhanced polarizability and heat transfer throughout the bulk sample. This behavior is evident up to 1000°C, where the dielectric constant for WBA is significantly higher compared to DBA, while the loss factor is lower. As described above, this can be correlated to changes in the electrical conductivity. The decrease in the slope of the dielectric constant of WBA above 1000°C, as found also for DBA, can be attributed to a combined reflection effect of graphite and metallic iron. The combined water and graphite addition is adequate to reduce the overall processing time to reach 1062 °C in 16 min for WBA, instead of 37 min for DBA (see Figs. 11 and 3). The addition of 25 wt% water shortens the initial heating up to 117°C prior to evaporation, whereas the graphite addition provides a more homogeneously heated product and eliminates the thermal runaway observed for DBA.

3.4. Penetration depth

The evolution of the microwave penetration depth in DBA and WBA was also investigated, as it directly affects the design of a microwave processing system and the feasibility of a potential scale-up asset. The penetration depth, i.e. the distance into the sample at which the electric field is attenuated to 1/e of its surface value, has been calculated using the eq. $D_p = \frac{\lambda_0 \sqrt{\varepsilon'}}{2\pi\varepsilon''}$ (where λ_0 is the wavelength of the microwave irradiation) and is presented in Fig. 13. Depending on the material, D_p can range between several micrometers for metals to several meters for low-loss materials such as Al_2O_3.

The high penetration depth in DBA below 320 °C indicates the limited potential of this material to absorb electromagnetic energy. At the onset temperature of pyrolysis and char production (320 °C), the penetration depth is reduced from 51.6 cm to 3.0 cm. This decrease is continued down to 0.3 cm throughout the 320–710 °C range, where the highest microwave absorption is expected. Comparison with WBA revealed an overall reduced penetration depth in WBA. In both cases, the lowest penetration depths are observed above 710 °C, with a minimum value of 0.9 cm for WBA at 822 °C.

The above observations indicate that the composition of the BA starting material strongly influences the microwave-material interaction, the concomitant thermal process as well as the microwave penetration depth into the product. All of these should be taken into account to judiciously design the most energy efficient microwave process for BA.

4. Conclusions

The response of MSWI BA to 2.45 GHz microwave irradiation was assessed through dielectric properties measurements up to 1060 °C. Dry BA is a low loss microwave absorber up to 320 °C, above which the dielectric properties are dominated by the pyrolysis of organic matter and the production of char resulting in an instantaneous thermal runaway of 500 °C/min. The identified phase changes in the BA during microwave processing were the formation of pyroxene group minerals, liquid phases and the gradual transformation of hematite to magnetite, wüstite and metallic iron.

Addition of 25 wt% water and 2 wt% graphite to the BA starting material substantially reduced the heating time from room temperature to 1062 °C from 36 to 16 min. The initial heating period up to the onset of pyrolysis was shortened due to the water addition, whereas the graphite addition allowed a controlled heating above 320 °C, avoiding an uncontrolled thermal runaway. At room temperature, 25 wt% water and 2 wt% graphite addition converts BA from a low loss material, with a loss tangent of 0.0051, to a medium loss material with increased loss tangent of 0.26. The microwave penetration depth in the water- and graphite-added BA was much smaller than in the pristine BA, especially below 320 °C. The penetration depth decreases with increasing temperature with a minimum of 0.9 cm around 800 °C.

Acknowledgments

This work was supported by the European Community's Horizon 2020 Programme under Grant Agreement No. 721185 (MSCA-ETN NEW-MINE). This publication reflects only the authors' view, exempting the Community from any liability. Project website: http://new-mine.eu/.

References

[1] Directive 2008/98/EC of the european parliament and of the council of 19 november 2008 on waste and repealing certain directives, http://data.europa.eu/eli/dir/2008/98/oj , Accessed date: 19 November 2008accessed.
[2] A.M. Joseph, R. Snellings, P. Van den Heede, S. Matthys, N. De Belie, The use of municipal solid waste incineration ash in various building materials: a Belgian point

of view, Materials 11 (2018), https://doi.org/10.3390/ma11010141.
[3] L. Bertolini, M. Carsana, D. Cassago, A.Q. Curzio, M. Collepardi, MSWI ashes as mineral additions in concrete, Cement Concr. Res. 34 (2004) 1899–1906, https://doi.org/10.1016/j.cemconres.2004.02.001.
[4] J. Born, Recycling Potentials of MSWI Bottom Ash EU Long Term Ambition : Legal Framework, 2014 http://www.cewep.eu/wp-content/uploads/2017/10/1318_avb_and_jp_born_2014_cewep_conference_bottom_ash_reuse.pdf.
[5] S.P.M. Berkhout, B.P.M. Oudenhoven, P.C. Rem, Optimizing non-ferrous metal value from MSWI bottom ashes, J. Environ. Prot. 02 (2011) 564–570, https://doi.org/10.4236/jep.2011.25065.
[6] R.C.C. Monteiro, S.J.G. Alendouro, F.M.L. Figueiredo, M.C. Ferro, M.H.V. Fernandes, Development and properties of a glass made from MSWI bottom ash, J. Non-Cryst. Solids 352 (2006) 130–135, https://doi.org/10.1016/j.jnoncrysol.2005.11.008.
[7] I. Znamenáčková, S. Dolinská, M. Kováčová, M. Lovás, V. Čablík, L. Čablíková, Innovative method of material treatmentby microwave energy, Proc. Earth Planet. Sci. 15 (2015) 855–860, https://doi.org/10.1016/j.proeps.2015.08.137.
[8] R. Taurino, A. Karamanov, R. Rosa, E. Karamanova, L. Barbieri, S. Atanasova-Vladimirova, G. Avdeev, C. Leonelli, New ceramic materials from MSWI bottom ash obtained by an innovative microwave-assisted sintering process, J. Eur. Ceram. Soc. 37 (2017) 323–331, https://doi.org/10.1016/j.jeurceramsoc.2016.08.011.
[9] A. Navarrete, R.B. Mato, G. Dimitrakis, E. Lester, J.R. Robinson, M.J. Cocero, S. Kingman, Measurement and estimation of aromatic plant dielectric properties. Application to low moisture rosemary, Ind. Crops Prod. 33 (2011) 697–703, https://doi.org/10.1016/j.indcrop.2011.01.012.
[10] F. Motasemi, M.T. Afzal, A.A. Salema, J. Mouris, R.M. Hutcheon, Microwave dielectric characterization of switchgrass for bioenergy and biofuel, Fuel 124 (2014) 151–157, https://doi.org/10.1016/j.fuel.2014.01.085.
[11] A.A. Salema, Y.K. Yeow, K. Ishaque, F.N. Ani, M.T. Afzal, A. Hassan, Dielectric properties and microwave heating of oil palm biomass and biochar, Ind. Crops Prod. 50 (2013) 366–374, https://doi.org/10.1016/j.indcrop.2013.08.007.
[12] A. Ilyas, M. Persson, M. Van Praagh, Dielectric properties of MSWI bottom ash for non-invasive monitoring of moisture, Environ. Monit. Assess. 185 (2013) 7053–7063, https://doi.org/10.1007/s10661-013-3085-7.
[13] R.M. Santos, G. Mertens, M. Salman, Ö. Cizer, T. Van Gerven, Comparative study of ageing, heat treatment and accelerated carbonation for stabilization of municipal solid waste incineration bottom ash in view of reducing regulated heavy metal/metalloid leaching, J. Environ. Manag. 128 (2013) 807–821, https://doi.org/10.1016/j.jenvman.2013.06.033.
[14] R.G. Duan, G. Roebben, J. Vleugels, O. Van der Biest, Stability of intergranular phases in hot-pressed Si3N4studied with mechanical spectroscopy and in-situ high-temperature XRD, J. Eur. Ceram. Soc. 22 (2002) 1897–1904, https://doi.org/10.1016/S0955-2219(01)00511-8.
[15] A.A. Coelho, TOPAS-academic, 2016, p. 208 Version 6: Technical Reference http://www.bruker-axs.de/.
[16] A. Belkly, M. Helderman, V.L. Karen, P. Ulkch, New developments in the inorganic crystal structure database (ICSD): accessibility in support of materials research and design, Acta Crystallogr. Sect. B Struct. Sci. 58 (2002) 364–369, https://doi.org/10.1107/S0108768102006948.
[17] L.F. Chen, C.K. Ong, C.P. Neo, V.V. Varadan, V.K. Varadan, Measurement of dielectric properties of materials at high temperatures, Microwave Electronics: Measurement and Materials Characterization, John Wiley & Sons, Ltd, New York, 2004, pp. 492–530, , https://doi.org/10.1002/0470020466.
[18] J.M. Catalá-Civera, A.J. Canós, P. Plaza-González, J.D. Gutiérrez, B. García-Baños, F.L. Peñaranda-Foix, Dynamic measurement of dielectric properties of materials at high temperature during microwave heating in a dual mode cylindrical cavity, IEEE Trans. Microw. Theory Tech. 63 (2015) 2905–2914, https://doi.org/10.1109/TMTT.2015.2453263.
[19] C.O. Kappe, How to measure reaction temperature in microwave-heated transformations, Chem. Soc. Rev. 42 (2013) 4977–4990, https://doi.org/10.1039/c3cs00010a.
[20] T. Durka, G.D. Stefanidis, T. Van Gerven, A. Stankiewicz, On the accuracy and reproducibility of fiber optic (FO) and infrared (IR) temperature measurements of solid materials in microwave applications, Meas. Sci. Technol. 21 (2010), https://doi.org/10.1088/0957-0233/21/4/045108.
[21] T. Durka, G.D. Stefanidis, T. Van Gerven, A.I. Stankiewicz, Microwave-activated methanol steam reforming for hydrogen production, Int. J. Hydrogen Energy 36 (2011) 12843–12852, https://doi.org/10.1016/j.ijhydene.2011.07.009.
[22] I. Lancellotti, C. Ponzoni, M.C. Bignozzi, L. Barbieri, C. Leonelli, Incinerator bottom ash and ladle slag for geopolymers preparation, Waste Biomass Valorization 5 (2014) 393–401, https://doi.org/10.1007/s12649-014-9299-2.
[23] F. Motasemi, A.A. Salema, M.T. Afzal, Dielectric characterization of corn stover for microwave processing technology, Fuel Process. Technol. 131 (2015) 370–375, https://doi.org/10.1016/j.fuproc.2014.12.006.
[24] J.P. Robinson, S.W. Kingman, R. Baranco, C.E. Snape, H. Al-Sayegh, Microwave pyrolysis of wood pellets, Ind. Eng. Chem. Res. 49 (2010) 459–463, https://doi.org/10.1021/ie901336k.
[25] M.H. and K.N. Masahiro Hotta, Complex Permittivity and Permeability of, 50 (2010) 1514–1516.
[26] B.S.L. Mcgill, W. Walkiewicz, Microwave Heating of Chemicals and Minerals, (1995).
[27] J.L. Rosenholtz, D.T. Smith, The dielectric constant of mineral powders, Am. Mineral. 21 (1936) 115–120 http://www.minsocam.org/ammin/AM21/AM21_115.pdf.
[28] T. Mason, Reanalysis of wustite electrical properties, Transport (1982) 24–26.
[29] J. Sun, W. Wang, Q. Yue, Review on microwave-matter interaction fundamentals and efficient microwave-associated heating strategies, Materials 9 (2016), https://doi.org/10.3390/ma9040231.
[30] J. El harfi, S.W. Kingman, G. Dimitrakis, J.P. Robinson, D.J. Irvine, Dielectric properties of free radical initiators—investigation of thermal decomposition products, Ind. Eng. Chem. Res. 51 (2012) 15811–15820, https://doi.org/10.1021/ie302076v.
[31] S. Chandrasekaran, T. Basak, R. Srinivasan, Microwave heating characteristics of graphite based powder mixtures, Int. Commun. Heat Mass Transf. 48 (2013) 22–27, https://doi.org/10.1016/j.icheatmasstransfer.2013.09.008.
[32] M. Shafi Khan, V.S. Chandel, R. Manohar, J.P. Shukla, Study of dielectric properties of fenugreek seeds (trigonella foenum graecum), Plant Breed. Seed Sci. 66 (2014), https://doi.org/10.2478/v10129-011-0054-6.
[33] V.V. Komarov, J. Tang, Dielectric permittivty and loss factor of tap water at 915 MHz, Microw. Opt. Technol. Lett. 42 (2004) 419–420, https://doi.org/10.1002/mop.20322.
[34] T.I. Sibianu, G. Dimitrakis, J. Katrib, C. Matei, D. Berger, C. Dodds, A.V. Surdu, I. Calinescu, D.J. Irvine, Utilization of dielectric properties assessment to evaluate the catalytic activity and rate of deactivation of heterogeneous catalysts, Ind. Eng. Chem. Res. 56 (2017) 1940–1947, https://doi.org/10.1021/acs.iecr.6b04341.